JACS Au
AN OPEN ACCESS JOURNAL OF THE AMERICAN CHEMICAL SOCIETY

pubs.acs.org/jacsau
Article

Zinc Oxide Nanoclusters Encapsulated in MFI Zeolite as a Highly Stable Adsorbent for the Ultradeep Removal of Hydrogen Sulfide

Tao Yu, Jinyu Zheng, Shikun Su, Yundong Wang,* Jianhong Xu,* and Zhendong Liu*

Cite This: *JACS Au* 2024, 4, 985−991
Read Online

ACCESS | Metrics & More | Article Recommendations | Supporting Information

ABSTRACT: Often, trace impurities in a feed stream will cause failures in industrial applications. The efficient removal of such a trace impurity from industrial steams, however, is a daunting challenge due to the extremely small driving force for mass transfer. The issue lies in an activity−stability dilemma, that is, an ultrafine adsorbent that offers a high exposure of active sites is favorable for capturing species of a low concentration, but free-standing adsorptive species are susceptible to rapidly aggregating in working conditions, thus losing their intrinsic high activity. Confining ultrafine adsorbents in a porous matrix is a feasible solution to address this activity−stability dilemma. We herein demonstrate a proof of concept by encapsulating ZnO nanoclusters into a pure-silica MFI zeolite (ZnO@silicalite-1) for the ultradeep removal of H_2S, a critical need in the purification of hydrogen for fuel cells. The Zn species and their interaction with silicalite-1 were thoroughly investigated by a collection of characterization techniques such as HADDF-STEM, UV−visible spectroscopy, DRIFTS, and ^{1}H MAS NMR. The results show that the zeolite offers rich silanol defects, which enable the guest nanoclusters to be highly dispersed and anchored in the silicious matrix. The nanoclusters are present in two forms, $Zn(OH)^+$ and ZnO, depending on the varying degrees of interaction with the silanol defects. The ultrafine nanoclusters exhibit an excellent desulfurization performance in terms of the adsorption rate and utilization. Furthermore, the ZnO@silicalite-1 adsorbents are remarkably stable against sintering at high temperatures, thus maintaining a high activity in multiple adsorption−regeneration cycles. The results demonstrate that the encapsulation of active metal oxide species into zeolite is a promising strategy to develop fast responsive and highly stable adsorbents for the ultradeep removal of trace impurities.

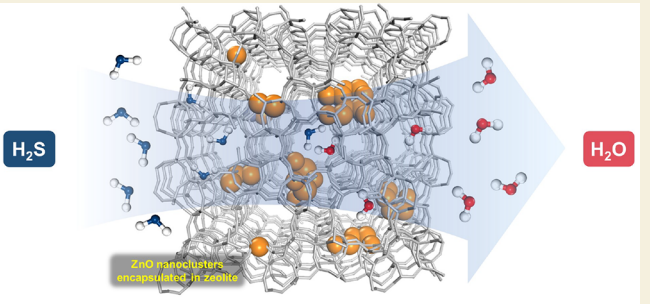

fast responsive and highly stable adsorbent for the ultradeep H_2S removal

KEYWORDS: *zeolite, nanoclusters, adsorption, H_2S removal, silanol defects*

INTRODUCTION

In many chemical processes, the purity of the feed matters, and even trace impurity may cause fatal failures such as contamination, corrosion, and catalyst deactivation. The ultradeep removal of trace impurities, however, is a daunting challenge. One apparent example is the purification of hydrogen for fuel cell applications. Hydrogen is a sustainable and clean energy, and currently, the hydrogen production from fossil resources (e.g., methane and coal) remains the most economically competitive compared with alternative routes.[1,2] Proton exchange membrane fuel cell (PEMFC) is a promising technique to utilize hydrogen to drive zero-emission vehicles.[3] As such, the purity of hydrogen has to be strictly controlled; particularly, contaminants such as H_2S and CO must be carefully removed, as H_2S and CO can easily deactivate platinum-based catalysts. For H_2S, the tolerance in hydrogen should be no higher than 0.004 ppm to ensure satisfactory performance and durability of PEM fuel cells.[4,5] Different desulfurization techniques have been developed over the decades, such as the Claus process and Rectisol process, to capture sulfur compounds from various streams; the combination of which is widely used in hydrogen purification to reduce the H_2S concentration to a certain degree. Further removal of the residual H_2S to meet the hydrogen specification for PEM fuel cells becomes infeasible due to the issue of equilibrium limitation. Physisorption-based pressure swing adsorption (PSA) is proposed as a technical alternative[6]; however, PSA not only requires a high energy input but also causes considerable hydrogen loss for reaching a satisfactory degree of desulfurization.

The challenge of ultradeep removal of trace impurities comes from both thermodynamic and kinetic aspects. Specific to H_2S, from the thermodynamics point of view, the sorbent (being adsorbent or absorbent) is required to have a high affinity with H_2S so as to achieve an ultradeep degree of

Received: November 21, 2023
Revised: February 15, 2024
Accepted: February 16, 2024
Published: March 1, 2024

desulfurization; whereas from the kinetics perspective, the adsorption/absorption process should take place at a reasonable pace even at a low H_2S concentration (or partial pressure), that is, with a small driving force for mass transfer. The above-mentioned Claus and Rectisol processes are insufficient to reduce H_2S concentration in the stream down to the parts-per-billion (ppb) level primarily due to the limitation in thermodynamics. Due to unique chemical properties, metal oxides have been widely studied and applied as adsorbents and catalysts.[7,8] Particularly, some metal oxides[9,10] (e.g., ZnO, CuO, and MnO) can react with H_2S to form metal sulfides, and this sulfidation reaction is thermodynamically favorable even at a very low H_2S concentration, making metal oxides a feasible class of adsorbents for the ultradeep H_2S removal. In fact, ZnO has been practiced as a H_2S adsorbent in the treatment of sour gas.[11] However, the conventional ZnO nanoparticles (tens of nanometers in general) are not efficient for the ultradeep removal of H_2S. The gas−solid sulfidation reaction over the ZnO nanoparticle is often diffusion-controlled, and the formation of a ZnS layer over ZnO further impedes the diffusion and sulfidation, which together result in that only limited external parts of the ZnO nanoparticle can participate in the sulfidation.[12] Ultrafine ZnO nanoclusters are thus favorable for the capture of low-concentration H_2S; yet, they are susceptible to severe sintering in high-temperature regeneration, losing the intrinsic high activity. Clearly, an activity−stability dilemma exists when exploring ultrafine ZnO nanoclusters for the ultradeep removal of trace H_2S (Scheme 1). Mesoporous silica has been attempted to confine metal oxide nanoparticles toward developing recyclable H_2S adsorbents.[13,14] Due to relatively large pore size and possibly weak interactions between metal oxide nanoparticles and mesoporous silica, however, apparent sintering and thereof degradation in adsorption capacity cannot be avoided. We thus envision that encapsulating ultrafine ZnO nanoclusters in a robust and microporous matrix can be a better solution to address the dilemma.

Scheme 1. Conceptual Illustration of the Preparation of Fast Responsive and Highly Stable Adsorbent for the Removal of Trace H_2S[a]

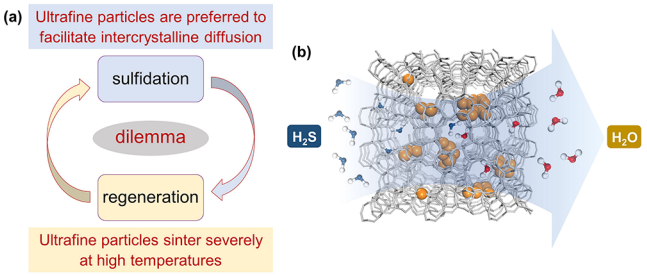

[a](a) The inherent dilemma between sulfidation and regeneration processes. (b) The concept of encapsulating ZnO nanoclusters into a zeolite matrix.

Zeolites are a class of crystalline microporous materials composed of tetrahedral (alumino)silicates. They possess remarkable properties, such as molecule-sized pores, tunable acidities, and unique shape selectivity, which enable them to play a critical role in chemical industries as adsorbents and catalysts.[15,16] Besides, zeolites offer plenty of nanospace to accommodate guest species of various forms, including single atoms, nanoclusters, and nanoparticles. Specifically, the encapsulation of metal nanoclusters into zeolites has drawn considerable research interest in recent years. The driving force for the encapsulation is mainly van der Waals interactions, that is, the physical confinement of nanoclusters from zeolite frameworks, which yields metal−zeolite composites that combine the high activity of ultrafine metal species and intrinsic features of zeolites. This combination has opened up a new avenue to design zeolite-based bifunctional catalysts that offer high activity, shape selectivity, and remarkable stability, as demonstrated in a number of examples. It is worth noting that, although considerable progress has been made in the field of catalysis, the potential of encapsulating active species into zeolites to create rapidly responsive and highly stable adsorbents for ultradeep removal of trace impurities has remained untapped.

As a proof of concept, we herein demonstrate that encapsulating ultrafine ZnO nanoclusters into a pure-silica MFI zeolite (silicalite-1) is a feasible route to develop highly active and exceptionally stable adsorbents for the ultradeep removal of trace H_2S (Scheme 1). To this end, we herein present the synthesis, characterizations, and H_2S adsorption assessments of the ZnO@silicalite-1 adsorbents. A particular focus is made to analyze the speciation and location of the ZnO nanoclusters, which allows us to understand how the ZnO nanoclusters interact with the zeolite matrix as well as how this interaction evolves in the adsorption−regeneration cycles. The results indicate that the silicliate-1 zeolite offers rich silanol defects serving as ideal anchors to confine uniformly dispersed ZnO nanoclusters of different forms, which enable the ZnO@silicalite-1 adsorbents to achieve high adsorption activity toward trace H_2S and maintain robust sintering-resistance in multiple adsorption−regeneration cycles. We believe this work showcases a promising strategy to develop highly selective, fast responsive, and remarkably stable adsorbent systems for the ultradeep removal of trace impurities.

RESULTS AND DISCUSSION

Properties and Performance of the Adsorbents

Silicalite-1, the pure-silica zeolite with an MFI structure, was chosen as the porous matrix because of its robust and inert framework; in addition, its 10-membered-ring pore openings, with a size of ca. 0.55 nm, allow H_2S to diffuse through the zeolite micropores to access the encapsulated adsorption sites. The synthesis of silicalite-1 was carried out following the procedure reported in a previous study. The resultant zeolite had a typical morphology of silicalite-1 synthesized from the classical TEOS-TPAOH-H_2O system, and the crystal size was about 400 nm (Figure S1). The encapsulation of the ZnO nanoclusters was done via wet impregnation of zinc nitrate into the silicalite-1 crystals followed by high-temperature calcination (see the Supporting Information). Three different ZnO loadings (1, 2, and 5 wt %, on the basis of the zeolite) were studied, and the samples were prepared by adjusting the zinc nitrate-to-zeolite ratio in the wet impregnation step. N_2 adsorption−desorption results (Figure S2 and Table S1) show that the micropore volume decreased with the loading of ZnO, indicating that the nanoclusters occupied the nanospace and consumed some of the micropore volume. The morphology and crystallinity of the zeolites, before and after

https://doi.org/10.1021/jacsau.3c00733
JACS Au 2024, 4, 985−991

the ZnO loading, were well maintained and almost identical, as shown in Figures S3 and S4, respectively. Particularly, no peaks due to ZnO could be identified from the XRD patterns, excluding the presence of any crystalline ZnO phases. Figure 1a–c displays the HAADF-STEM images of the ZnO@

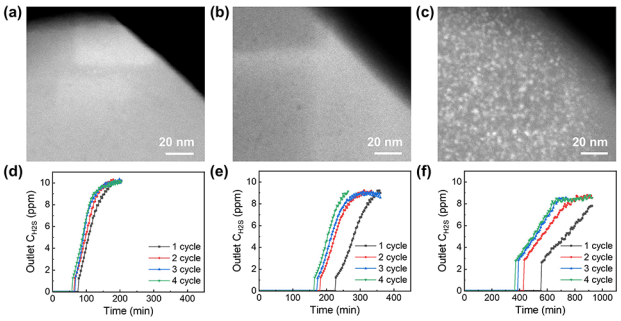

Figure 1. ZnO@silicalite-1 adsorbents and their performances in trace H_2S removal. (a–c) HAADF-STEM images of 1 wt % ZnO@silicalite-1, 2 wt % ZnO@silicalite-1, and 5 wt % ZnO@silicalite-1, respectively; (d–f) H_2S breakthrough curves during consecutive four adsorption–regeneration cycles for 1 wt % ZnO@silicalite-1, 2 wt % ZnO@silicalite-1, and 5 wt % ZnO@silicalite-1, respectively (the inlet H_2S concentration was 10 ppm, and the adsorption and regeneration temperatures were 150 and 500 °C, respectively).

silicalite-1 adsorbents with different ZnO loadings. At low loadings (1 and 2 wt %), almost no apparent nanoclusters can be seen. Note that there is a small difference in terms of *Z* contrast between Zn and Si, which makes it challenging to differentiate between Zn and Si with HAADF-STEM if one element is present as small-sized nanoclusters and highly dispersed in the other one. As such, we conclude that the ZnO nanoclusters were highly dispersed and of too small size to be clearly identified at lower ZnO loadings. With further increasing the ZnO loading to 5 wt %, the nanoclusters become clearly visible by HAADF-STEM. The image in Figure 1c depicts that the nanoclusters were of ca. 2 nm in size and homogeneously distributed in the zeolite matrix. No apparent white spots over the edge of the zeolite can be seen from the HAADF-STEM, suggesting that there was no enrichment of nanoclusters on the external surface of the zeolite.

Adsorption tests were conducted to assess the capability as well as the recyclability of the ZnO@silicalite-1 adsorbents in the removal of low-concentration H_2S. The procedure of the adsorption tests can be found in Figure S5. The H_2S concentration in the effluent was monitored by using a gas chromatograph (GC) equipped with a flame photometric detector (FPD). As the gas injection to GC was done every 2 min, and due to a small amount of adsorbent in the bed, there was a sudden increase of H_2S concentration from non-detectable to a certain number at the point of breakthrough. From the breakthrough curves in Figure 1d–f, we can see that the ZnO@silicalite-1 adsorbents exhibited varying H_2S adsorption capacities, reflecting that the sulfidation of zinc oxides into metal sulfides did take place although the ZnO species were encapsulated by the zeolite matrix. The adsorption capacity of the ZnO@silicalite-1 adsorbents increased reasonably with ZnO loading. It is worth noting that the ZnO@silicalite-1 adsorbents exhibited remarkable recyclability, with a high adsorption capacity preserved after four sulfidation–regeneration cycles. The high recyclability is attributed to the fact that the effective confinement of the ZnO nanoclusters by the zeolite matrix rendered them highly sinter-resistant against high temperatures, which will be discussed in detail later. In contrast, a commercial ZnO adsorbent composed of free-standing nanoparticles lost 70% of its initial adsorption capacity after the first regeneration, primarily due to severe sintering at the high temperature (Figure S6). With 5 wt % ZnO loaded, the regenerated ZnO@silicalite-1 adsorbent much outperformed the regenerated ZnO nanoparticles by giving a doubled adsorption capacity. These results justify the merits of encapsulating ZnO nanoclusters in zeolites for the ultradeep removal of H_2S.

Investigation of the Zinc Speciation

We characterized the ZnO@silicalite-1 adsorbents in detail to probe the ZnO speciation as well as to understand how the ZnO species interact with the zeolite. Figure 2a shows the

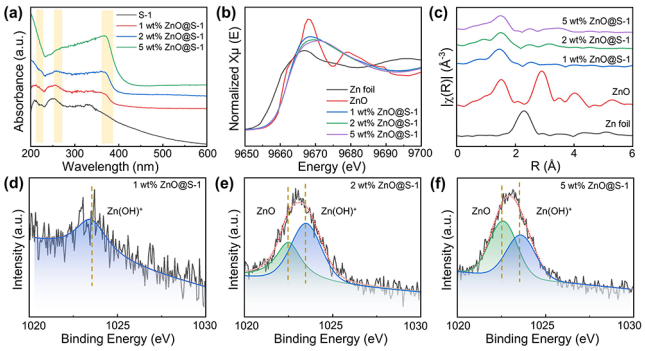

Figure 2. Characterization of ZnO@silicalite-1 adsorbents with different ZnO loadings. (a) UV–visible diffuse spectra of ZnO@silicalite-1 with different ZnO loadings. (b) Zn *k*-edge XANES spectra of ZnO@silicalite-1 with different ZnO loadings. (c) Fourier transform of the k^2-weighted EXAFS spectra with different ZnO loadings. (d–f) Zn $2p_{3/2}$ XPS spectra of ZnO@silicalite-1 with different ZnO loadings ("ZnO@silicalite-1" was abbreviated as "ZnO@S-1" for clarity in the figures).

diffuse reflectance UV–vis spectra of the host silicalite-1 zeolites and ones encapsulated with varying loadings of ZnO. Only a weak absorption feature around 200 nm can be observed, which suggests that the extraframework zinc species dominated in the ZnO@silicalite-1 samples. The absorption band at ca. 370 nm could probably be attributed to nanocrystalline ZnO, the intensity of which increases reasonably with the ZnO loading.[17] The previous reports by Haase et al. demonstrated that there exists a blue shift in the UV–vis absorption spectra of ZnO particles if the size decreases to the order of the Bohr radius.[17−20] Accordingly, the absorption band at ca. 270 nm could be assigned to ZnO nanoclusters with sizes of less than 1 nm. XAS measurements were conducted to probe the state and composition of Zn species. Figure 2b shows the Zn *k*-edge XANES spectra of the ZnO@silicalite-1 samples together with those from bulk ZnO and the Zn foil references. All the ZnO@silicalite-1 samples exhibit an apparent absorption feature at 9961.8 eV, which is in consistent with absorption feature of the ZnO standard reference. Figure 2c depicts the Fourier transforms of the EXAFS spectra k^2 weighted over the *k* range from 2.3 to 11.0 $Å^{-1}$. An apparent feature of the first-shell distance in the range of 1.0–2.0 Å can be seen from the ZnO@silicliate-1 samples, which is ascribed to the Zn–O backscattering. Besides, a feature at ca. 2.6 Å possibly arising from the Zn–Si

https://doi.org/10.1021/jacsau.3c00733
JACS Au 2024, 4, 985–991

backscattering is also observed.[21,22] The XAS data collectively demonstrate that divalent zinc species dominated in the samples, which is fairly reasonable, as there should be no occurrence of self-reduction to generate any atomic zinc species. Although the valence state of the zinc species was unaffected by the loading, the Zn $2p_{3/2}$ XPS results (Figure 2d–f) indicate that the zinc species exhibited different interactions with the zeolite framework depending on the amount. At a low zinc loading (Figure 2d), only a weak peak centered at ca. 1023.6 eV is detected, which is assumed to be zinc oxide in its hydroxide form, $Zn(OH)^+$. The presence of in ZSM-5 has been confirmed in previous studies by XPS along with other spectroscopic tools.[23,24] Although the pure-silica zeolite is theoretically neutral, silicalite-1 actually exhibits a certain electronegativity due to the existence of abundant defects, which thus create a microenvironment to accommodate the $Zn(OH)^+$ species.[25,26] The other peak centered at ca. 1022.6 eV, which corresponds to ZnO, started to appear in Figure 2e, and its relative intensity with respect to that of the peak at 1023.6 eV increased with the zinc loading (Figure 2f).[18,27−29] The XPS results indicate that the framework oxygen in the zeolite could exert a higher electronegativity toward zinc in the $Zn(OH)^+$ species than that between oxygen ligand and zinc in the species of ZnO nanoclusters.[23,24] This loading-dependent interaction between the zinc species and zeolite is consistent with previous studies of zinc-containing ZSM-5 zeolites.

To further probe the interactions between the zinc species and zeolite, we carried out diffuse reflectance infrared Fourier transform spectroscopy (DRIFTS) and ^{1}H solid-state magic-angel spinning nuclear magnetic resonance (MAS NMR) measurements to analyze the changes of the microenvironment in the pure-silica MFI zeolite. The previous works claimed that the ZSM-5 zeolite could not accommodate ZnO nanocrystalline species larger than 1 nm, which would instead appear on the external surface of the zeolite if present. As for the pure-silica MFI zeolite in our study, nevertheless, we found that the rich defective environments can play a critical role in the encapsulation of ZnO species of different types and sizes. Because the parent zeolite was synthesized using TPAOH as an organic structure-directing agent, it contained various silanol groups,[30,31] as seen from the DRIFT spectra of the parent zeolite and ones encapsulated with ZnO (Figure S7). The bands at 3740 and 3510 cm^{-1} correspond to isolated silanols located on the external surface and silanol nests inside the silicalite-1 zeolite, respectively. Besides, the band at ca. 3730 cm^{-1} could correspond to terminal silanols inside the zeolite.[32−34] When loading of Zn species, the band at 3740 cm^{-1} weakens; while the one at 3510 cm^{-1} decreases apparently, implying that the ZnO species occupied the silanol nests and made their vibrations less detectable. Furthermore, we note that, when the ZnO content reached to 5 wt %, a new band at 3680 cm^{-1} appeared, which is probably associated with the formation of Zn−OH on the surface.[32] In further, qualitative analysis of the silanol defects was obtained from the ^{1}H MAS NMR measurements. Due to large diversity of the hydroxyl groups in terms of geometry and proximity, the silanol defects in the silicalite-1 exhibit very complex hydrogen-bonding abilities.[35] According to previous models obtained from a combination of DFT calculation and spectroscopic studies, two types of silanols can be identified from the ^{1}H MAS NMR spectra (Type I and Type II in Figure 3a)[30]: the chemical shift in the range of ca. 1.2−2.8 ppm is assigned to the Type I silanols, which have lower possibility to form hydrogen bonds, whereas the chemical shift in the range of ca. 2.8−8.5 ppm is assigned to the Type II silanols, which exhibit medium and strong hydrogen-bonding abilities. Detailed peak assignments are given in the Supporting Information. The deconvolution result in Figure 3b shows that the proportion values of Type I silanols and that of Type II silanols were 34.19 and 65.81%, respectively, in the parent zeolite. From Figure 3c–e, we observe a decreasing trend of the Type II silanols when the ZnO species were encapsulated, and correspondingly, the relative amount of the Type I silanols increased. The results suggest that the Type II silanol groups tend to capture the ZnO species in between, thus reducing the possibility of forming hydrogen bonds.

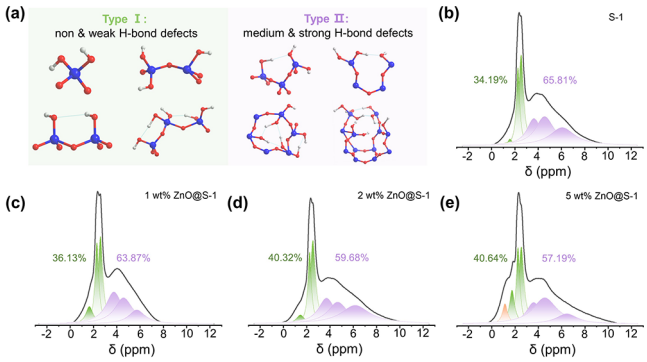

Figure 3. Interaction between the zinc species and zeolite. (a) Schematic illustration of different types of silanols and hydrogen bonds formed; (b–e) ^{1}H MAS NMR spectra of silicalite-1, 1 wt % ZnO@silicalite-1, 2 wt % ZnO@silicalite-1, and 5 wt % ZnO@silicalite-1, respectively ("ZnO@silicalite-1" was abbreviated as "ZnO@S-1" for clarity in the figures).

Based on the analyses of the ZnO speciation as well as the interaction between the ZnO species and silanol groups, we propose the states and microenvironments of the encapsulated ZnO species in the silicalite-1 zeolite (Figure 4). At a low ZnO

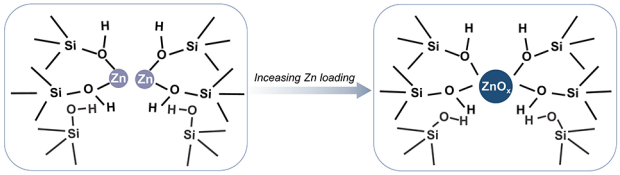

Figure 4. Schematic illustration of the interactions between the Zn species and zeolite. At a low ZnO loading, the zinc species tend to be highly dispersed and are mainly present in the form of hydroxide oxide. With the increase of ZnO loading, zinc oxide with a higher nuclearity is formed.

loading, where the silanol groups in the zeolite are relatively rich, the zinc species tend to be highly dispersed and mainly present in the form of hydroxide oxide. With the increasing of ZnO loading, more zinc species enter the silanol groups and thus form zinc oxide with a higher nuclearity. In either case, the zinc species closely interact with the silanol groups (in particularly, the Type II silanols), which explains the high dispersion of the ZnO nanoclusters as well as their high stability against sintering at high temperatures.

https://doi.org/10.1021/jacsau.3c00733
JACS Au 2024, 4, 985−991

Evolution of the Zinc Species during Sulfidation–Regeneration Cycles

The sulfidated and regenerated ZnO@silicalite-1 adsorbents were characterized to track the evolution of the ZnO species in multiple sulfidation and regeneration cycles. According to the TEM images in Figure S8, no apparent aggregation of the ZnO species is observed from the sulfidated and regenerated samples, indicating that the adsorbents were remarkably sintering-resistant against the high-temperature regeneration. The ^{1}H MAS NMR spectra of the sulfidated and regenerated ZnO@silicalite-1 adsorbents (Figure 5) show that a large

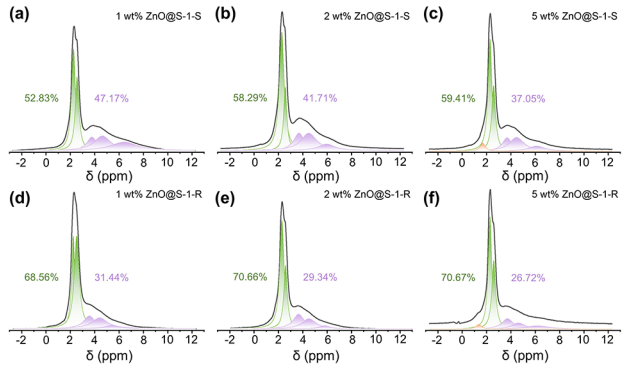

Figure 5. Evolution of different types of silanols during the sulfidation and regeneration cycles. (a–c) ^{1}H MAS NMR spectra of sulfidated ZnO@silicalite-1 with different ZnO loadings. (d–f) ^{1}H MAS NMR spectra of regenerated ZnO@silicalite-1 after 4 sulfidation–regeneration cycles with different ZnO loadings. (Note: "ZnO@S-1" represents "ZnO@silicalite-1", "ZnO@S-1-S" represents "sulfidated ZnO@silicalite-1", and "ZnO@S-1-R" represents "regenerated ZnO@silicalite-1 after four sulfidation–regeneration cycles").

number of the silanol defects were preserved in the sulfidation–regeneration cycle. The preservation of silanol defects is also confirmed by the DRIFT results in Figures S9 and S10.

We note that the relative amount of Type II silanols decreased after the sulfidation and that the declining tendency was more apparent with the increase of ZnO loading. It was reported that self-healing of zeolite defects can take place in an aqueous solution,[36,37] where water molecules could mediate the migration and condensation of silanol groups. Since H_2S is an acid gas, it is likely that the H_2S molecules, albeit of low concentration, could to some extent behave similarly as H_2O molecules to induce the partial condensation of the silanols. It is interesting to observe that there was considerable presence of the Type II silanols in the ZnO@silicaliate-1 adsorbents even after four cycles of sulfidation and regeneration, with the latter performed at 500 °C for 4 h. We also performed a control experiment in which the parent zeolite was further calcined at 500 °C for different periods of time. The result in Figure S11 shows that the proportion of Type II silanols decreased with the calcination period and that they almost disappeared after the calcination for 10 h because of condensation at high temperatures. This comparison implies that the ZnO species could help prevent the silanol groups against condensation at high temperatures. With above results, we come to a conclusion that the interaction between the guest ZnO species and parent zeolite is 2-fold: the zeolite offers rich silanol defects as ideal anchors to encapsulate the ZnO nanoclusters, rendering them to be homogeneously dispersed in the zeolite and behave highly active and sintering-resistant in the H_2S adsorption; meanwhile, the encapsulated ZnO nanoclusters segregate the silanol groups, which reduces their chances of condensation at high temperatures.

CONCLUSIONS

In summary, we put forward a new concept to design adsorbents that are capable of overcoming the activity–stability dilemma in the ultradeep removal of trace impurities. This concept involves encapsulating metal oxide nanoclusters as chemisorption-active sites into a robust zeolite matrix. We demonstrated a validation of this concept by confining ZnO nanoclusters into a pure-silica MFI zeolite and proved that the ZnO@silicalite-1 adsorbents were highly active and exceptionally stable in the ultradeep removal of H_2S. The detailed characterization results showed that the zeolite offered rich defective sites to anchor the ZnO nanoclusters and that the interaction between the guest ZnO nanoclusters and parent zeolite played a critical role in the stabilization of the ultrafine ZnO nanoclusters. Although zeolites feature remarkable (hydrothermal) stability, the diffusion limitation due to their intrinsic micropores might be a concern. To overcome this issue, we also demonstrated that it could be possible to encapsulate the ZnO nanoclusters into a hollow silicalite-1 zeolite (Figure S12). The ultrafine ZnO nanoclusters were uniformly dispersed in the thin shell (with a thickness of ca. 20 nm) of the hollow zeolite, thus greatly reducing the diffusion distance. The hollow adsorbent exhibited a fast response in the ultradeep removal of H_2S as well as reasonable stability against sintering at high temperatures. On the basis of the collective results, we believe our work offers a promising strategy to develop highly selective, fast responsive, and remarkably stable adsorbent systems that are of particular significance to the ultradeep removal of trace impurities.

ASSOCIATED CONTENT

Supporting Information

The Supporting Information is available free of charge at https://pubs.acs.org/doi/10.1021/jacsau.3c00733.

Detailed descriptions of experimental procedures, XRD patterns, SEM images, and other supporting characterization results (PDF)

AUTHOR INFORMATION

Corresponding Authors

Yundong Wang – *State key Laboratory of Chemical Engineering, Department of Chemical Engineering, Tsinghua University, Beijing 100084, China*; Email: wangyd@tsinghua.edu.cn

Jianhong Xu – *State key Laboratory of Chemical Engineering, Department of Chemical Engineering, Tsinghua University, Beijing 100084, China*; Email: xujianhong@tsinghua.edu.cn

Zhendong Liu – *State key Laboratory of Chemical Engineering, Department of Chemical Engineering, Tsinghua University, Beijing 100084, China*; orcid.org/0000-0002-3364-2523; Email: liuzd@tsinghua.edu.cn

https://doi.org/10.1021/jacsau.3c00733
JACS Au 2024, 4, 985–991

Authors

Tao Yu − *State key Laboratory of Chemical Engineering, Department of Chemical Engineering, Tsinghua University, Beijing 100084, China*

Jinyu Zheng − *Sinopec Research Institute of Petroleum Processing Co., LTD., Beijing 100083, China*

Shikun Su − *Sinopec Research Institute of Petroleum Processing Co., LTD., Beijing 100083, China*

Complete contact information is available at: https://pubs.acs.org/10.1021/jacsau.3c00733

Notes

The authors declare no competing financial interest.

■ ACKNOWLEDGMENTS

This work was supported in part by National Natural Science Foundation of China (grants: 22278237, 22178196), a Sinopec fund (no.: 122096), State Key Laboratory of Chemical Engineering (grant no.: SKL-ChE-22T04), and a start-up fund (to Z.L.) from Tsinghua University.

■ REFERENCES

(1) Zheng, B.; Wang, S.; Xu, J. A Review on the CO2 Emission Reduction Scheme and Countermeasures in China's Energy and Power Industry under the Background of Carbon Peak. *Sustainability* **2022**, *14* (2), 879.

(2) Vasilakos, P. N.; Shen, H.; Mehdi, Q.; Wilcoxen, P.; Driscoll, C.; Fallon, K.; Burtraw, D.; Domeshek, M.; Russell, A. G. US Clean Energy Futures—Air Quality Benefits of Zero Carbon Energy Policies. *Atmosphere* **2022**, *13* (9), 1401.

(3) Lü, X.; Qu, Y.; Wang, Y.; Qin, C.; Liu, G. A Comprehensive Review on Hybrid Power System for PEMFC-HEV: Issues and Strategies. *Energy Conversion and Management* **2018**, *171*, 1273−1291.

(4) Cheng, X.; Shi, Z.; Glass, N.; Zhang, L.; Zhang, J.; Song, D.; Liu, Z.-S.; Wang, H.; Shen, J. A Review of PEM Hydrogen Fuel Cell Contamination: Impacts, Mechanisms, and Mitigation. *J. Power Sources* **2007**, *165* (2), 739−756.

(5) https://www.iso.org/standard/69539.html.

(6) Mergenthal, M.; Tawai, A.; Amornraksa, S.; Roddecha, S.; Chuetor, S. Methane Enrichment for Biogas Purification Using Pressure Swing Adsorption Techniques. *Mater. Today: Proc.* **2023**, *72*, 2915−2920.

(7) Salavati-Niasari, M.; Dadkhah, M.; Davar, F. Pure Cubic ZrO2 Nanoparticles by Thermolysis of a New Precursor. *Polyhedron* **2009**, *28* (14), 3005−3009.

(8) Mir, N.; Salavati-Niasari, M. Preparation of TiO2 Nanoparticles by Using Tripodal Tetraamine Ligands as Complexing Agent via Two-Step Sol−Gel Method and Their Application in Dye-Sensitized Solar Cells. *Mater. Res. Bull.* **2013**, *48* (4), 1660−1667.

(9) Cimino, S.; Lisi, L.; Erto, A.; Deorsola, F. A.; de Falco, G.; Montagnaro, F.; Balsamo, M. Role of H2O and O2 during the Reactive Adsorption of H2S on CuO-ZnO/Activated Carbon at Low Temperature. *Microporous Mesoporous Mater.* **2020**, *295*, No. 109949.

(10) Chytil, S.; Kure, M.; Lødeng, R.; Blekkan, E. A. Performance of Mn-Based H2S Sorbents in Dry, Reducing Atmosphere − Manganese Oxide Support Effects. *Fuel* **2017**, *196*, 124−133.

(11) Gibson, J. B.; Harrison, D. P. The Reaction between Hydrogen Sulfide and Spherical Pellets of Zinc Oxide. *Ind. Eng. Chem. Proc. Des. Dev.* **1980**, *19* (2), 231−237.

(12) Neveux, L.; Chiche, D.; Bazer-Bachi, D.; Favergeon, L.; Pijolat, M. New Insight on the ZnO Sulfidation Reaction: Evidences for an Outward Growth Process of the ZnS Phase. *Chemical Engineering Journal* **2012**, *181−182*, 508−515.

(13) Elyassi, B.; Wahedi, Y. A.; Rajabbeigi, N.; Kumar, P.; Jeong, J. S.; Zhang, X.; Kumar, P.; Bal-asubramanian, V. V.; Katsiotis, M. S.; Andre Mkhoyan, K.; Boukos, N.; Hashimi, S. A.; Tsapatsis, M. A High-Performance Adsorbent for Hydrogen Sulfide Removal. *Microporous Mesoporous Mater.* **2014**, *190*, 152−155.

(14) Fan, B.; Zhao, W.; Ghosh, S.; Mkhoyan, K. A.; Tsapatsis, M.; Stein, A. Diffusive Formation of Hollow Mesoporous Silica Shells from Core−Shell Composites: Insights from the Hydrogen Sul-fide Capture Cycle of CuO@mSiO2 Nanoparticles. *Langmuir* **2020**, *36* (23), 6540−6549.

(15) Zhang, Q.; Gao, S.; Yu, J. Metal Sites in Zeolites: Synthesis, Characterization, and Catalysis. *Chem. Rev.* **2022**, *123*, 6039.

(16) Dusselier, M.; Van Wouwe, P.; Dewaele, A.; Jacobs, P. A.; Sels, B. F. Shape-Selective Zeolite Catalysis for Bioplastics Production. *Science* **2015**, *349* (6243), 78−80.

(17) Chen, J.; Feng, Z.; Ying, P.; Li, C. ZnO Clusters Encapsulated inside Micropores of Zeolites Studied by UV Raman and Laser-Induced Luminescence Spectroscopies. *J. Phys. Chem. B* **2004**, *108* (34), 12669−12676.

(18) Geng, R.; Liu, Y.; Guo, Y.; Wang, P.; Dong, M.; Wang, S.; Wang, J.; Qin, Z.; Fan, W. Structure Evolution of Zn Species on Fresh, Deactivated, and Regenerated Zn/ZSM-5 Catalysts in Ethylene Aromatization. *ACS Catal.* **2022**, *12* (23), 14735−14747.

(19) Shen, X.; Kang, J.; Niu, W.; Wang, M.; Zhang, Q.; Wang, Y. Impact of Hierarchical Pore Structure on the Catalytic Performances of MFI Zeolites Modified by ZnO for the Conversion of Methanol to Aromatics. *Catal. Sci. Technol.* **2017**, *7* (16), 3598−3612.

(20) Haase, M.; Weller, H.; Henglein, A. Photochemistry and Radiation Chemistry of Colloidal Semiconductors. 23. Electron Storage on Zinc Oxide Particles and Size Quantization. *J. Phys. Chem.* **1988**, *92* (2), 482−487.

(21) Zhao, D.; Gao, M.; Tian, X.; Doronkin, D. E.; Han, S.; Grunwaldt, J.-D.; Rodemerck, U.; Linke, D.; Ye, M.; Jiang, G.; Jiao, H.; Kondratenko, E. V. Effect of Diffusion Constraints and ZnOx Speciation on Nonoxidative Dehydrogenation of Propane and Isobutane over ZnO-Containing Catalysts. *ACS Catal.* **2023**, *13* (5), 3356−3369.

(22) Zhang, B.; Li, G.; Zhai, Z.; Chen, D.; Tian, Y.; Yang, R.; Wang, L.; Zhang, X.; Liu, G. PtZn Intermetallic Nanoalloy Encapsulated in Silicalite-1 for Propane Dehydrogenation. *AIChE J.* **2021**, *67* (7), No. e17295.

(23) Gong, T.; Qin, L.; Lu, J.; Feng, H. ZnO Modified ZSM-5 and Y Zeolites Fabricated by Atomic Layer Deposition for Propane Conversion. *Phys. Chem. Chem. Phys.* **2016**, *18* (1), 601−614.

(24) Tamiyakul, S.; Ubolcharoen, W.; Tungasmita, D. N.; Jongpatiwut, S. Conversion of Glycerol to Aromatic Hydrocarbons over Zn-Promoted HZSM-5 Catalysts. *Catal. Today* **2015**, *256*, 325−335.

(25) Xie, L.; Wang, R.; Chai, Y.; Weng, X.; Guan, N.; Li, L. Propane Dehydrogenation Catalyzed by In-Situ Partially Reduced Zinc Cations Confined in Zeo-lites. *Journal of Energy Chemistry* **2021**, *63*, 262−269.

(26) Liu, X.; Lv, X.; Song, W.; Zhang, G.; Guo, X. Regioselective Distribution of Zinc Hydroxyl within Straight Channels in MFI Zeolite Nanosheets for Propane Dehydrogenation. *Ind. Eng. Chem. Res.* **2024**, *63*, 121.

(27) Han, S.; Zhao, D.; Otroshchenko, T.; Lund, H.; Bentrup, U.; Kondratenko, V. A.; Rockstroh, N.; Bartling, S.; Doronkin, D. E.; Grunwaldt, J.-D.; Rodemerck, U.; Linke, D.; Gao, M.; Jiang, G.; Kondratenko, E. V. Elucidating the Nature of Active Sites and Fundamentals for Their Creation in Zn-Containing ZrO2 − Based Catalysts for Nonoxidative Propane Dehydrogenation. *ACS Catal.* **2020**, *10* (15), 8933−8949.

(28) Gabrienko, A. A.; Arzumanov, S. S.; Toktarev, A. V.; Danilova, I. G.; Prosvirin, I. P.; Kriventsov, V. V.; Zaikovskii, V. I.; Freude, D.; Stepanov, A. G. Different Efficiency of Zn2+ and ZnO Species for Methane Activation on Zn-Modified Zeolite. *ACS Catal.* **2017**, *7* (3), 1818−1830.

(29) Niu, X.; Gao, J.; Miao, Q.; Dong, M.; Wang, G.; Fan, W.; Qin, Z.; Wang, J. Influence of Preparation Method on the Performance of Zn-Containing HZSM-5 Catalysts in Methanol-to-Aromatics. *Microporous Mesoporous Mater.* **2014**, *197*, 252−261.

(30) Dib, E.; Costa, I. M.; Vayssilov, G. N.; Aleksandrov, H. A.; Mintova, S. Complex H-Bonded Silanol Network in Zeolites Revealed by IR and NMR Spectroscopy Combined with DFT Calculations. *J. Mater. Chem. A* **2021**, *9* (48), 27347−27352.
(31) Palčić, A.; Moldovan, S.; El Siblani, H.; Vicente, A.; Valtchev, V. Defect Sites in Zeolites: Origin and Healing. *Adv. Sci.* **2022**, *9* (4), No. 2104414.
(32) Liu, J.; Liu, Y.; Liu, H.; Fu, Y.; Chen, Z.; Zhu, W. Silicalite-1 Supported ZnO as an Efficient Catalyst for Direct Propane Dehydrogenation. *ChemCatChem.* **2021**, *13* (22), 4780−4786.
(33) Liu, G.; Liu, J.; He, N.; Miao, C.; Wang, J.; Xin, Q.; Guo, H. Silicalite-1 Zeolite Acidification by Zinc Modification and Its Catalytic Properties for Isobutane Conversion. *RSC Adv.* **2018**, *8* (33), 18663−18671.
(34) Amiri, M.; Salavati-Niasari, M.; Akbari, A.; Gholami, T. Removal of Malachite Green (a Toxic Dye) from Water by Cobalt Ferrite Silica Magnetic Nanocomposite: Herbal and Green Sol-Gel Autocombustion Synthesis. *Int. J. Hydrogen Energy* **2017**, *42* (39), 24846−24860.
(35) Dubray, F.; Dib, E.; Medeiros-Costa, I.; Aquino, C.; Minoux, D.; van Daele, S.; Nesterenko, N.; Gilson, J.-P.; Mintova, S. The Challenge of Silanol Species Characterization in Zeolites. *Inorg. Chem. Front.* **2022**, *9* (6), 1125−1133.
(36) Prodinger, S.; Derewinski, M. A.; Vjunov, A.; Burton, S. D.; Arslan, I.; Lercher, J. A. Improving Stability of Zeolites in Aqueous Phase via Selective Removal of Structural Defects. *J. Am. Chem. Soc.* **2016**, *138* (13), 4408−4415.
(37) Iyoki, K.; Kikumasa, K.; Onishi, T.; Yonezawa, Y.; Chokkalingam, A.; Yanaba, Y.; Matsumoto, T.; Osuga, R.; Elangovan, S. P.; Kondo, J. N.; Endo, A.; Okubo, T.; Wakihara, T. Extremely Stable Zeolites Developed via Designed Liquid-Mediated Treatment. *J. Am. Chem. Soc.* **2020**, *142* (8), 3931−3938.

https://doi.org/10.1021/jacsau.3c00733
JACS Au 2024, 4, 985−991